Semiclassical initial value theory of rotationally inelastic scattering: Some remarks on the phase index in the interaction picture

L. Bonnet[*,†,‡]

† *Université de Bordeaux, ISM, UMR 5255, F-33400 Talence, France*

‡ *CNRS, ISM, UMR 5255, F-33400 Talence, France*

E-mail: \markcomm{black}{claude-laurent.bonnet@u-bordeaux.fr}

Abstract

This paper deals with the treatment of quantum interferences in the semiclassical initial value theory of rotationally inelastic scattering in the interaction picture [C. W. McCurdy and W. H. Miller, J. Chem. Phys. **67**, 463 (1977)]. It is shown that substituting the original phase index by a new one extends the range of applicability of the theory. The resulting predictions are in close agreement with exact quantum scattering results for a model of atom-rigid diatom collision involving strong interferences. The developments are performed within the framework of the planar rotor model, but they are readily applicable to the three-dimensional case.

1   Introduction

Numerous calculations performed over the last two decades[1–25] have shown that the classical trajectory method[1,26–29] generally allows the nearly quantitative description of the dynamics and the kinetics of molecular processes relevant to atmospherical and interstellar chemistry. These calculations may require quantum corrections to improve their accuracy, like the use of Wigner distributions,[14,30] one-dimensional tunneling probabilities,[31–36] Gaussian binning,[8,13] surface hopping,[37–41] etc., but contrary to semiclassical calculations,[42–55] they do not assign probability amplitudes and phases to classical paths. In this regard, the classical trajectory method mostly ignores the wave character of nuclear motions involved in molecular processes.

Sometimes, however, these calculations are "too classical" and lack of realism. This is typically the case for rotationally inelastic atom-diatom collisions, of great importance in interstellar chemistry[56] and stereodynamics.[57–65] Unlike chemical reactions, inelastic collisions may involve strong interference effects that are only partially (if not at all) quenched by the summation over total and orbital (or helicity) quantum numbers involved in the calculation of integral cross sections (ICS). This is typically the case for collisions of near-homonuclear (almost symmetrical) molecules such as NO with noble gasses.[57–65] For such

processes, interference effects show up in final rotational state distributions, or in the steric asymmetry measuring the dependence of the previous distributions on the initial orientation of the diatom with respect to the atom (quantum expectations oscillate about classical ones).

In an illuminating analysis, McCurdy and Miller[66] showed within a planar model of atom-diatom inelastic collision that the semiclassical theory of molecular collision[42–55] not only reproduces the previous interference features, but also provides deep insight into their physical origin. The primary reason for this success is that, as previously stated, semiclassical methods assign probability amplitudes and phases to classical trajectories and make them interfere, respecting thereby the quantum principle of superposition. The accuracy with which one makes these paths interfere is the subject of this report.

It should be noted that for atom-diatom inelastic collisions, exact quantum scattering (EQS) calculations are nearly routine nowadays.[67–69] Moreover, the promizing implementation of the mixed quantum/classical theory by Semenov and Babikov[70–73] may also provide accurate results at a lower computational cost. These benchmark calculations, however, are often too complex to provide insight into the physics underlying interference effects. The main interest of the semiclassical approach of inelastic collisions is thus its explicative power.

One may thus wonder why this approach has never been used to reproduce and analyze the state-of-the-art stereodynamics measurements performed over the last two decades.[57–65] This is likely due to major and somehow discouraging numerical difficulties encountered in the application of semiclassical scattering methods, especially when the dynamics involves trapped trajectories.[53] However, the processes under scrutiny in stereodynamical studies[57–65] involve a single rebound mechanism and hence, no trapping. For such type of encounters, at least two previous works by Miller[74] and Campolieti and Brumer[49] suggest that realistic (full-dimensional) semiclassical calculations should be feasible.

In principle, accurate semiclassical (SC) predictions are expected to be obtained within the *initial value representation* (IVR) discovered by Miller,[43] and first applied to vibrationally inelastic collisions. This method is developed within the *interaction picture*, as we

3

shall see further below. The major interests of the SCIVR approach are twofold. First, it allows to go round the root-search issue of *classical S-matrix theory* (CSMT),[42–44] mother of all semiclassical methods of molecular scattering. Second, it is able to predict quantum mechanically allowed transitions that are classically forbidden, contrary to CSMT. For rotationally inelastic collisions, Miller's SCIVR S-matrix elements are given by Eq. (3.5) in Ref.[66] for the planar rotor, and Eq. (12) in Ref.[49] for the three-dimensional rotor. The goal of this work is to increase the range of applicability of these expressions by considering a phase index different from the original one. The developments are performed within the framework of the planar rotor model, but they can be straightforwardly extended to the three-dimensional case.

The paper is laid out as follows. The previously outlined SCIVR method[66] is presented and applied to a model of atom-planar rotor collision in Sec. . Three coupling strengths between translational and rotational motions are considered. For the two lowest ones, SCIVR predictions are in close agreement with EQS results, but for the strongest one, clear disagreement is found. In order to shed light on this finding, the conditions of validity of the SCIVR method are analyzed in Sec. . In particular, we show that the latter does not necessarily lead to CSMT in the classical limit. This inconsistency is removed in Sec. by modifying the phase index. SCIVR predictions are then in close agreement with EQS results for the three coupling strengths. A technical discussion follows in Sec. and Sec. concludes.

2 SCIVR theory in the interaction picture

We consider, within a fixed-plane of the laboratory frame, the collision between an atom and a rigid diatom rotating in the previous plane. Moreover, both the atom and the center-of-mass of the rotor are supposed to move on a fixed line of the plane throughout the collision (see Fig. 1 in Ref.[54]). Detailed discussions of the classical, semiclassical and quantum dynamics of this collisional system can be found elsewhere.[46,54,55] Calling R the distance between the atom and the center-of-mass of the rotor, ϕ the Jacobi angle and P and J their

respective conjugate momenta, the classical Hamiltonian of the system is given by

$$H = H_0 + V(R, \phi) \tag{1}$$

where

$$H_0 = \frac{P^2}{2\mu} + \frac{J^2}{2I} \tag{2}$$

is the unperturbed Hamiltonian. μ is the reduced mass of the atom-diatom system. I is the moment of inertia of the diatom, given by

$$I = mr^2 \tag{3}$$

were m is the reduced mass of the diatom and r its bond length. $V(R, \phi)$ is the interaction potential. In addition to ϕ, we introduce the shifted Jacobi angle

$$\tilde{\phi} = \phi - \frac{\mu R J}{PI}. \tag{4}$$

$\mu R/P$ is the time to go from 0 to R when ignoring the interaction between the atom and the diatom, i.e., when assuming that the dynamics is governed by H_0 instead of H. Moreover, J/I is the angular velocity of the rotor. $\mu R J/(PI)$ is thus the variation of ϕ when going from 0 to R if the Hamiltonian of the system is H_0. Hence, $\tilde{\phi}$ results from making ϕ evolve forward in time according to H and then backward in time according to H_0. This evolution is analogous to that of a quantum state in the interaction picture.[75] Note that $\tilde{\phi}$ is a constant of motion in the asymptotic channel where $V(R, \phi)$ is zero.

Let $S_{j_2 j_1}(E)$ be the probability amplitude to go from the initial rotational state j_1 to the final state j_2 at the total energy E. The set of trajectories used further below to calculate this element is defined as follows. They are started at R_1, large enough for $V(R, \phi)$ to be negligible, with $H = E = H_0$ (see Eq. (1)). Moreover, the initial angular momentum J_1 of the rotor is kept at $\hbar j_1$. From Eq. (2), we thus have

$$P_1 = -\left[2\mu\left(H_0 - \frac{J_1^2}{2I}\right)\right]^{1/2} = -\left[2\mu\left(E - \frac{\hbar^2 j_1^2}{2I}\right)\right]^{1/2}. \tag{5}$$

The initial shifted angle $\tilde{\phi}_1$ can take any value within the range $[0, 2\pi]$. The resulting trajectories cross the interaction region and eventually come back to the asymptotic channel. They are finally stopped at R_2, large enough for $V(R, \phi)$ to be negligible. The values of $\tilde{\phi}$ and J at R_2 are denoted $\tilde{\phi}_2$ and J_2, respectively. Since both $\tilde{\phi}$ and J are constants of motion in the asymptotic channel, $\tilde{\phi}_2$ and J_2 are their final values. From Eq. (2), we have

$$P_2 = \left[2\mu\left(E - \frac{J_2^2}{2I}\right)\right]^{1/2}. \tag{6}$$

We note from Eq. (4) and the left equality of Eq. (5) that

$$\left.\frac{\partial X_2}{\partial \tilde{\phi}_1}\right|_{J_1} = \left.\frac{\partial X_2}{\partial \phi_1}\right|_{J_1} \tag{7}$$

with X_2 equal J_2 or $\tilde{\phi}_2$. This identity will be useful in the following.

Miller's SCIVR expression of $S_{j_2 j_1}(E)$ reads

$$S_{j_2 j_1}(E) = \frac{1}{2\pi i}\int_0^{2\pi} d\tilde{\phi}_1 \left(\left.\frac{\partial \tilde{\phi}_2}{\partial \tilde{\phi}_1}\right|_{J_1}\right)^{1/2} e^{i\Phi/\hbar} \tag{8}$$

6

with

$$\Phi = (J_2 - \hbar j_2)\, \tilde{\phi}_2 + \Omega \tag{9}$$

and

$$\Omega = -\int_0^t d\tau \left(R\dot{P} + \phi \dot{J} \right) \tag{10}$$

(see Eq. (3.5) in Ref.[66]; the only difference is that in the present Eq. (8), an overall and arbitrary phase factor $1/i$ has been added for consistency with previous developments,[54] and $\hbar$ is not kept at 1). The partial derivative $\frac{\partial \tilde{\phi}_2}{\partial \tilde{\phi}_1}\big|_{J_1}$ is deduced from the set of trajectories previously introduced and a second batch of nearby paths starting with the same initial conditions but slightly different values of $\tilde{\phi}_1$. Eq. (8) can be rewritten as

$$S_{j_2 j_1}(E) = \frac{1}{2\pi i} \int_0^{2\pi} d\tilde{\phi}_1 \left| \frac{\partial \tilde{\phi}_2}{\partial \tilde{\phi}_1} \right|_{J_1}^{1/2} e^{i(\Phi/\hbar - \pi\nu/2)}. \tag{11}$$

The phase index ν is equal to 0 if $\frac{\partial \tilde{\phi}_2}{\partial \tilde{\phi}_1}\big|_{J_1}$ is positive. In the contrary case, ν is equal to ± 1. The two signs are considered since the form of the pre-exponential factor in Eq. (8) does not allow to decide which branch of the square root should be chosen. The calculations performed by means of this first index will be called SC-I$^-$ and SC-I$^+$ for $\nu = (0, -1)$ and $(0, +1)$, respectively.

The model planar collision used to check the validity of Eq. (8) is governed by H with[54]

$$V(R, \phi) = exp\left[-\alpha \left(R - \beta cos\phi \right) \right]. \tag{12}$$

7

While α is fixed at 2 Å^{-1}, β is taken at the three different values 0.1, 0.3, and 1.02 Å corresponding to increasing couplings between the R and ϕ coordinates in the interaction region. E is kept at 0.5 eV, j_1 at 0, μ at 2/3 amu, m at 1/2 amu and r at 1 Å. R_1 and R_2 are both taken at 4 Å, beyond which $V(R, \phi)$ is negligibly small and the integrand in Eq. (11) is a constant of motion. The collisional systems resulting from the previous parameters involve strong interferences, as shown by the exact quantum state distributions $P_{j_2 j_1}(E) = |S_{j_2 j_1}(E)|^2$ displayed in Fig. 1 (blue circles connected by dotted segments; see Ref. [54] for some details on their calculations). Since $J_1 = 0$, we note from Eq. (4) that $\tilde{\phi}_1 = \phi_1$.

For $\beta = 0$, there is no coupling between R and ϕ and J keeps constantly equal to $\hbar j_1$ during the collision. Calling $t(R_1, R_2)$ the time to go from R_1 to the interaction region and back to R_2, we have

$$\phi_2 = \phi_1 + \frac{\hbar j_1}{I} \, t(R_1, R_2). \tag{13}$$

Using Eq. (4), we thus arrive at

$$\tilde{\phi}_2 = \phi_1 + \frac{\hbar j_1}{I} \, t(R_1, R_2) - \frac{\mu R_2 \hbar j_1}{P_1 I} \tag{14}$$

with P_1 given by Eq. (5). From Eqs. (7) and (14), and the fact that $t(R_1, R_2)$ does not depend on ϕ_1, we obtain

$$\left. \frac{\partial \tilde{\phi}_2}{\partial \tilde{\phi}_1} \right|_{J_1} = 1. \tag{15}$$

$\left. \frac{\partial \tilde{\phi}_2}{\partial \tilde{\phi}_1} \right|_{J_1}$ is represented in Fig. 2 for $\beta = 0$ and the three values previously considered. For β equal 0.1, the coupling is small and $\left. \frac{\partial \tilde{\phi}_2}{\partial \tilde{\phi}_1} \right|_{J_1}$ slightly oscillates around 1. For β equal 0.3, the coupling is stronger, thus leading to oscillations around 1 of larger amplitude. In both cases, however, $\left. \frac{\partial \tilde{\phi}_2}{\partial \tilde{\phi}_1} \right|_{J_1}$ is found to be positive. Hence, the SC-I$^-$ and SC-I$^+$ approaches lead

to the same results, simply labeled SC-I (green squares connected by solid segments in the upper and middle panels of Fig. 1). As a matter of fact, the agreement between quantum and semiclassical predictions is very satisfying.

On the other hand, for β equal 1.02, the strength of the coupling is such that $\frac{\partial \tilde{\phi}_2}{\partial \tilde{\phi}_1}\big|_{J_1}$ can take both signs. The SC-I$^-$ and SC-I$^+$ approaches then lead to different results (green squares and brown diamonds connected by solid segments in the lower panel of Fig. 1). Both of them appear to be in quantitative disagreement with EQS results as compared to the two previous cases. In Sec. , we determine the origin of this problem and in Sec. , we show how to fix it.

3   Condition of validity of Eq. (11)

Let us momentarily abandon Eq. (11) to concentrate on CSMT,[42–44] the "most classical" semiclassical approach of molecular collisions. The CSMT expression of $S_{j_2 j_1}(E)$ reads

$$
S_{j_2 j_1}(E) = \sum_k \left(\frac{2\pi i}{\hbar} \left| \frac{\partial J_2}{\partial \tilde{\phi}_1} \right|_{J_1}^k \right)^{-1/2} e^{i(\Omega_k/\hbar - \pi \eta_k/2)} \tag{16}
$$

(we assume here that $i^{1/2} = e^{i\pi/4}$). The sum is over the discrete set of trajectories starting from R_1 with P_1 given by the right-hand-side (RHS) of Eq. (5) and reaching R_2 with $J_2 = \hbar j_2$. The new quantity appearing here is η_k, the Maslov index[76] of the classical Green function, equal here to the number of caustics touched by the kth trajectory. These are located as follows; a second path is considered, starting from the same point (R_1, ϕ_1^k) as the kth trajectory, but with initial momenta differing by an infinitely small amount from those of the kth trajectory (with the constraint $H_0 = E$ still satisfied). The kth trajectory touches a caustic the instant it is crossed by the second path in the (R, ϕ) plane. The practical calculation of η_k is detailed in section II.A.3 of ref.[54]. In the same work, two trajectories involving one and two caustics are schematically represented in Figs. 5 and 6, respectively.

They correspond to the blue lines. The green lines in the lower panels are the second paths, crossing the blue lines once (Fig. 5) or twice (Fig. 6). It is demonstrated below these figures that $\frac{\partial J_2}{\partial \tilde{\phi}_1}\big|_{J_1}$ is positive (negative) for one (two) caustic(s). This finding will be useful in the following. A detailed derivation of Eq. (16) from first principles can be found in Refs.[54,55]. Eq. (16) above is identical to Eq. (103) in Ref.[54], where g is in fact equal to 1[55] and $\frac{\partial J_2}{\partial \phi_1}\big|_{J_1}^{k}$ replaces $\frac{\partial J_2}{\partial \tilde{\phi}_1}\big|_{J_1}^{k}$, a substitution justified by Eq. (7).

CSMT is the theory toward which any kind of SCIVR approach is expected to converge in the classical limit.[43,49,52,54] Hence, one should recover Eq. (16) from Eq. (11) when making $\hbar$ tend to 0 in the latter. Note, however, that the resulting expression may differ from the RHS of Eq. (16) by an irrelevant phase factor, noted $e^{i\pi l/2}$ without loss of generality, disappearing when considering $|S_{j_2 j_1}(E)|^2$. In order to introduce the standard result of asymptotic analysis necessary to perform the passage from Eq. (11) to Eq. (16), consider two functions f and g, the former involving N stationary points $(x_1, ..., x_N)$. For an infinitely small parameter s (we take it positive), it can be shown that

$$\int dx \, g(x) e^{if(x)/s} = \sum_{k=1}^{N} g(x_k) \left(\frac{2\pi i s}{|f''(x_k)|} \right)^{1/2} e^{i[f(x_k)/s - \pi \chi_k/2]} \tag{17}$$

where χ_k is 0 if $f''(x_k)$ is positive, 1 otherwise.[77] When applied to the case where s is small but not negligible with respect to the $|f''(x_k)|$'s, Eq. (17) is known as the *stationary phase approximation* (SPA). We now use it to integrate the RHS of Eq. (11) over $\tilde{\phi}_1$. First of all, we rewrite Eq. (10) as

$$\Omega = - \int_{P_1}^{P_2} R dP - \int_{\hbar j_1}^{J_2} \phi dJ. \tag{18}$$

Since only the upper bounds P_2 and J_2 depend on $\tilde{\phi}_1$, we have

$$\left. \frac{\partial \Omega}{\partial \tilde{\phi}_1} \right|_{J_1} = -R_2 \left. \frac{\partial P_2}{\partial \tilde{\phi}_1} \right|_{J_1} - \phi_2 \left. \frac{\partial J_2}{\partial \tilde{\phi}_1} \right|_{J_1}. \tag{19}$$

Using the fact that P_2 and J_2 satisfy Eq. (2) (with $H_0 = E$) and using Eq. (4) allows to rewrite Eq. (19) as

$$\left. \frac{\partial \Omega}{\partial \tilde{\phi}_1} \right|_{J_1} = -\tilde{\phi}_2 \left. \frac{\partial J_2}{\partial \tilde{\phi}_1} \right|_{J_1}, \tag{20}$$

which, together with Eq. (9), leads to

$$\left. \frac{\partial \Phi}{\partial \tilde{\phi}_1} \right|_{J_1} = (J_2 - \hbar j_2) \left. \frac{\partial \tilde{\phi}_2}{\partial \tilde{\phi}_1} \right|_{J_1} \tag{21}$$

and

$$\left. \frac{\partial^2 \Phi}{\partial \tilde{\phi}_1^2} \right|_{J_1} = \left. \frac{\partial J_2}{\partial \tilde{\phi}_1} \right|_{J_1} \left. \frac{\partial \tilde{\phi}_2}{\partial \tilde{\phi}_1} \right|_{J_1} + (J_2 - \hbar j_2) \left. \frac{\partial^2 \tilde{\phi}_2}{\partial \tilde{\phi}_1^2} \right|_{J_1}. \tag{22}$$

Therefore, the values of $\tilde{\phi}_1$ making Φ stationary are those leading to

$$J_2 = \hbar j_2 \tag{23}$$

or

$$\left. \frac{\partial \tilde{\phi}_2}{\partial \tilde{\phi}_1} \right|_{J_1} = 0. \tag{24}$$

11

From Eqs. (11), (17) and (22), we finally arrive at

$$S_{j_2 j_1}(E) = \sum_k \left(\frac{2\pi i}{\hbar} \left| \frac{\partial J_2}{\partial \tilde{\phi}_1} \right|_{J_1}^k \right| \right)^{-1/2} e^{i(\Omega_k/\hbar - \pi(\nu_k + \chi_k)/2)}. \tag{25}$$

The sum is over those trajectories satisfying Eq. (23). Since the prefactor of the integrand in Eq. (11) is $\left| \frac{\partial \tilde{\phi}_2}{\partial \tilde{\phi}_1} \right|_{J_1}^{1/2}$, it is clear from Eqs. (11), (17) and (22) that the contribution to $S_{j_2 j_1}(E)$ of those trajectories complying with Eq. (24) is zero. We thus recover Eq. (16), but with the index η_k replaced by $\nu_k + \chi_k$. As previously stated, the RHS of Eqs. (16) and (25) may differ by an irrelevant phase factor $e^{i\pi l/2}$. Multiplying the latter by the RHS of Eq. (16) and equating the resulting product with the RHS of Eq. (25) leads to the condition for the validity of Eq. (11), namely

$$\eta_k = \nu_k + \chi_k + l. \tag{26}$$

For clarity's sake, we recall that (i) η_k is the number of caustics touched by the trajectories, (ii) ν_k is 0 if $\frac{\partial \tilde{\phi}_2}{\partial \tilde{\phi}_1} \big|_{J_1}$ is positive, ± 1 otherwise, and (iii) χ_k is 0 if $\frac{\partial J_2}{\partial \tilde{\phi}_1} \big|_{J_1} \frac{\partial \tilde{\phi}_2}{\partial \tilde{\phi}_1} \big|_{J_1}$ is positive, 1 otherwise. l is thus necessarily an integer.

We now want to know when Eq. (26) is satisfied. To answer this question, 36 trajectories projected onto the (R, ϕ) plane are represented in Fig. 3 for $\beta = 0.3$. Trajectories initially come from the right with $J_1 = 0$ and are thus parallel to the R-axis. They rebound against the anisotropic potential wall which rotationally excites the diatom (except for $\phi_1 = 0$ and π). The final directions of the rotationally excited trajectories make a non zero angle with the R-axis. All the trajectories, indigo plus green, touch a first caustic, represented by a blue thick line lying within the interaction region. On the other hand, only the green paths touch a second caustic, represented by a red thick line. η_k is thus equal to 1 for the indigo paths, and 2 for the green paths. Moreover, we have previously seen that $\frac{\partial \tilde{\phi}_2}{\partial \tilde{\phi}_1} \big|_{J_1}$ is always

positive for $\beta = 0.3$ (see Fig. 2), thus implying $\nu_k = 0$. Hence, we deduce from the definition of χ_k (see above) that $\chi_k = 0$ if $\frac{\partial J_2}{\partial \tilde{\phi}_1}\big|_{J_1}$ is positive, 1 otherwise. Now, we have seen previously that $\frac{\partial J_2}{\partial \tilde{\phi}_1}\big|_{J_1}$ is positive (negative) for one (two) caustic(s). Consequently, $\chi_k = 0$ when $\eta_k = 1$ while $\chi_k = 1$ when $\eta_k = 2$. Eq. (26) is thus satisfied whatever $\tilde{\phi}_1$ if l is taken at 1. This scenario holds for $\beta = 0.1$.

On the other hand, the situation is more complex for $\beta = 1.02$ as trajectories touch up to three caustics. The difference between η_k and $\nu_k + \chi_k$ is found to strongly vary in terms of $\tilde{\phi}_1$ for both definitions of ν_k [(0,+1) or (0,-1)]. As a consequence, Eq. (26) cannot be satisfied whatever $\tilde{\phi}_1$ with a single value of l. A sufficiently small coupling between translational and rotational motions within the interaction region appears to be a prerequisite for the validity of Eq. (11).

4 Alternative phase index

Eq. (26) suggests the expression of the index making general Eq. (11). It is indeed sufficient to replace ν by $\eta - \chi - l$ in Eq. (11). Thanks to this substitution, the latter will necessarily lead to Eq. (16) within the SPA. Related developments have been performed by Campolieti and Brumer in order to derive phase indices for various SCIVR time-dependent propagators.[78] Since only the relative phases of S-matrix elements are relevant, the value of l is irrelevant. Taking it at 0 leads to

$$S_{j_2 j_1}(E) = \frac{1}{2\pi i} \int_0^{2\pi} d\tilde{\phi}_1 \left| \frac{\partial \tilde{\phi}_2}{\partial \tilde{\phi}_1} \right|_{J_1} \right|^{1/2} e^{i(\Phi/\hbar - \pi(\eta - \chi)/2)}. \tag{27}$$

A slightly different alternative to this expression, suggested by previous developments,[54,55] is

$$S_{j_2 j_1}(E) = \frac{1}{2\pi i} \int_0^{2\pi} d\tilde{\phi}_1 \left| \frac{\pi_2}{P_2} \frac{\partial \tilde{\phi}_2}{\partial \tilde{\phi}_1} \right|_{J_1} \right|^{1/2} e^{i(\Phi/\hbar - \pi(\eta - \chi)/2)}, \tag{28}$$

where π_2 is given by Eq. (6) with $J_2 = \hbar j_2$. The advantage of Eq. (28) over Eq. (27) is that $S_{j_2 j_1}(E)$ is rigorously zero for energetically prohibited transitions. Within the SPA, however, both expressions lead to Eq. (16). The rotational state distributions obtained by means of Eq. (28), labeled SC-II, are compared with EQS distributions in Fig. 4. For β equal 0.1 and 0.3, things are obviously unchanged with respect to Fig. 1, but for β equal 1.02, the agreement between semiclassical and quantum calculations is considerably improved. Eq. (27) leads to virtually identical results.

5   Discussion

The *sine qua non* condition for obtaining accurate semiclassical predictions from Eqs. (27) or (28) is that R_2 is taken in principle at infinity, in practice at a large value (at least $\sim 10^2$ Å). The reason is as follows. For $\beta = 0.3$, the value of $log(R)$ at the caustics is represented in terms of ϕ_1 in Fig. 5. The blue and red curves correspond, respectively, to the blue and red caustics in Fig. 3. If one takes R_2 at ~ 10 Å, as is commonly done in classical trajectory calculations, the Maslov index η is found equal to 1 for all the trajectories crossing the red caustic beyond ~ 10 Å, i.e., for all the paths such that $log(R)$ is larger than ~ 1 (see Fig. 5). This is a wrong estimation since $\eta = 2$ for these paths. Though the latter represent a small percentage of the whole set of trajectories contributing to S-matrix elements (see Fig. 5), the alteration of the rotational state distribution is significant, as seen in Fig. 6. Total disagreement is found for $R_2 = 4$ Å, value for which the purely classical predictions, or the semiclassical ones according to Eq. (11), are already converged. To get the red curve in Fig. 5, it was necessary to take R_2 at 10^2 Å. For obtaining the rotational distributions, however, such calculations are not only heavy, they are useless. It is sufficient to run trajectories up to 4 Å, and then to analytically deduce the trajectory conditions at any larger value of R_2 (we took it at 10^3) from those at 4 Å. On the other hand, there is no need to take R_1 at a large value, since the first caustic (blue line in Fig. 3) lies within the interaction region. R_1

was thus taken at 4 Å for all the calculations related to this work.

The value of the norm $[\Sigma = \Sigma_{j_2} P_{j_2 j_1}(E)]$ is an excellent criterion of accuracy. The closer to 1, the more accurate the semiclassical predictions. In a first series of calculations, we found that for 1800 trajectories, Eq. (28) leads to $\Sigma = 0.9999$ for $\beta = 0.1$ (only the significant digits are given), $\Sigma = 0.999$ for $\beta = 0.3$ and $\Sigma = 1.02$ for $\beta = 1.02$. Eq. (27) leads to nearly identical predictions. One notes that the accuracy decreases with the coupling strength between the R and ϕ coordinates, i.e., when trajectories become more and more unstable. In a second series of calculations, we sought to determine the minimum number of trajectories maintaining the previous accuracy. For $\beta = 0.1$ and 0.3, we arrived at the amazingly low numbers of 16 and 30, respectively. These numbers are of the order of those found in previous studies.[52,66] This is far less than the number of trajectories necessary to estimate final state distributions by means of the classical trajectory method which totally misses interferences ! On the other hand, a much larger number of 660 trajectories is mandatory for $\beta = 1.02$. When β increases, calculations are more time-consuming in addition to be less accurate.

The fact that a few tens of trajectories may be enough for accurate semiclassical predictions on inelastic collisions involving one rotational degree-of-freedom (DOF) augurs well for the extension of the present work to realistic atom-rigid diatom collisions involving two rotational DOFs. For such processes, Miller's SCIVR S-matrix elements are indeed given by integrals over the two angles conjugate to j and l, respectively.[49] For nearly isotropic potential energy surfaces such as those involved in stereodynamics studies, and for given initial values (j_1, l_1) of (j, l), $\sim 10^3$ trajectories (the square of 30) should be enough for converging the calculation of $S^J_{j_2 l_2, j_1 l_1}$, where J is now the total angular momentum, and j_2 and l_2 can take any values consistent with the conservation of E and J. For $j_1 = 0$, a few tens of thousands of trajectories are expected to be sufficient to obtain the ICS, and hence, the steric asymmetry. Note that the analytical extrapolation of the dynamics from a few Å to infinity is feasible for an atom-rigid diatom system.

A few years ago, several SCIVR approaches of rotational transitions were proposed within

the standard configuration space coordinates (R, ϕ)[54,55]. These formulations all involve phase indices making them in principle of general applicability. Unfortunately, however, they also involve integrals of functions oscillating all the more as R_1 and R_2 take large values, making thereby challenging the numerical convergence of S-matrix elements in the asymptotic channel. Eqs. (27) and (28) do not suffer from this drawback, for their integrands do not depend on R_1 and R_2 in the asymptotic channel (apart from η which we know how to calculate).

Amazingly accurate SCIVR calculations have been performed by Elran and Kay.[52] To date, however, their approach has only been applied to collinear processes, and its applicability to three-dimensional collisions is an open issue.[52] Moreover, the mathematical form of their S-matrix elements is much more complex than the one of Eqs. (27) and (28). It is thus unclear whether this approach can be used to explain quantum interferences as efficiently as Eqs. (27) or (28). This is all the more so as the previous equations already provide quasi-quantitative results (see Fig. 4).

6 Conclusion

Miller's SCIVR theory in the interaction picture[66] (Eq. (11)) was presented and applied to a model of atom-planar rotor inelastic collision involving strong quantum interferences. Three coupling strengths between translational and rotational motions were considered. For the two lowest ones, SCIVR predictions were found to be in close agreement with quantum scattering results. For the strongest one, however, clear disagreement was observed. In order to shed light on this finding, the conditions of validity of Eq. (11) were analyzed. We found that the latter tends to classical S-matrix theory[42–44] in the classical limit only whether the coupling strength is sufficiently small. This inconsistency was removed by substituting a new phase index to the original one. SCIVR predictions were then found to be in close agreement with quantum scattering results whatever the coupling strength. The next step will be to apply the present work to the realistic case of three-dimensional rotationally inelastic collisions. In the event that the resulting approach provides accurate predictions,

we will have a powerful tool at our disposal to better analyze rotational state distributions of astrochemical interest,[56] or the state-of-the-art stereodynamics measurements currently performed.[62–65]

References

(1) Aoiz, F.; Banares, L.; Herrero, V. Recent results from quasiclassical trajectory computations of elementary chemical reactions. *J. Chem. Soc. Faraday Trans.* **1998**, *94*, 2483.

(2) Aoiz, F. J.; Banares, L.; Castillo, J. F.; Herrero, V. J.; Martínez-Haya, B.; Honvault, P.; Launay, J. M.; Liu, X.; Lin, J. J.; Harich, S. A. et al. The O(^{1}D)+ H$_2$ reaction at 56 meV collision energy: A comparison between quantum mechanical, quasiclassical trajectory, and crossed beam results. *J. Chem. Phys.* **2002**, *116*, 10692.

(3) Banares, L.; Aoiz, F. J.; Honvault, P.; Bussery-Honvault, B.; Launay, J.-M. Quantum mechanical and quasi-classical trajectory study of the C(^{1}D)+ H$_2$ reaction dynamics. *J. Chem. Phys.* **2003**, *118*, 565.

(4) Kim, M.; Moon, J. Development of classical trajectory methodology for the study of dissociation dynamics of polyatomic ions. *Int. J. Mass Spec.* **2003**, *225*, 191.

(5) Townsend, D.; Lahankar, S. A.; Lee, S. K.; Chambreau, S. D.; Suits, A. G.; Zhang, X.; Rheinecker, J.; Harding, L. B.; Bowman, J. M. The Roaming Atom: Straying from the Reaction Path in Formaldehyde Decomposition. *Science* **2004**, *306*, 1158.

(6) Xie, T.; Bowman, J.; Duff, J.; Braunstein, M.; Ramachandran, B. Quantum and quasiclassical studies of the O(^{3}P) + HCl $\longrightarrow$ OH+ Cl(^{2}P) reaction using benchmark potential surfaces. *J. Chem. Phys.* **2005**, *122*, 014301.

(7) Aoiz, F. J.; Banares, L.; Herrero, V. J. Dynamics of Insertion Reactions of H$_2$ Molecules with Excited Atoms. *J. Phys. Chem. A* **2006**, *110*, 12546.

(8) González-Martínez, M. L.; Bonnet, L.; Larrégaray, P.; Rayez, J.-C. Classical treatment of molecular collisions: striking improvement of the description of recoil energy distributions using Gaussian weighted trajectories. *J. Chem. Phys.* **2007**, *126*, 041102.

(9) Sierra, J. D.; Bonnet, L.; Gonzalez, M. Quasi-Classical Trajectory-Gaussian Binning Study of the OH + $D_2 \longrightarrow$ HOD(v_1', v_2', v_3') + D Angle-Velocity and Vibrational Distributions at a Collision Energy of 0.28 eV. *J. Phys. Chem. A* **2011**, *115*, 7413.

(10) Czakó, G.; Wang, Y.; Bowman, J. Communication: Quasiclassical trajectory calculations of correlated product-state distributions for the dissociation of $(H_2O)_2$ and $(D_2O)_2$. *J. Chem. Phys.* **2011**, *135*, 151102.

(11) Li, Z.; Xie, C.; Jiang, B.; Xie, D.; Liu, L.; Sun, Z.; Zhang, D. H.; Guo, H. Quantum and quasiclassical state-to-state dynamics of the NH + H reaction: Competition between abstraction and exchange channels. *J. Chem. Phys.* **2011**, *134*, 134303.

(12) Bonnet, L.; Larrégaray, P.; Arbelo-González, W.; de Castro-Vítores, M. Normalization of the Gaussian binning trajectory method for indirect reactions. *Comp. Theor. Chem.* **2012**, *30*, 990.

(13) Bonnet, L. Classical dynamics of chemical reactions in a quantum spirit. *Int. Rev. Phys. Chem.* **2013**, *32*, 171.

(14) Arbelo-Gonzalez, W.; Bonnet, L.; García-Vela, A. New insights into the semiclassical Wigner treatment of photodissociation dynamics. *Phys. Chem. Chem. Phys.* **2013**, *15*, 9994.

(15) Czakó, G.; Bowman, J. M. Reaction Dynamics of Methane with F, O, Cl, and Br on ab Initio Potential Energy Surfaces. *J. Phys. Chem. A* **2014**, *118*, 2839.

(16) Szabó, P.; Lendvay, G. A Quasiclassical Trajectory Study of the Reaction of H Atoms with $O_2(^1\Delta_g)$. *J. Phys. Chem. A* **2015**, *119*, 7180.

(17) Braunstein, M.; Conforti, P. Classical Dynamics of H_2O Vibrational Self-Relaxation. *J. Phys. Chem. A* **2015**, *119*, 3311.

(18) Shao, K.; Fu, B.; Zhang, D. H. A global full-dimensional potential energy surface and quasiclassical trajectory study of the $O(^1D) + CH_4$ multichannel reaction. *Phys. Chem. Chem. Phys.* **2015**, *17*, 24098.

(19) Esposito, F.; Coppola, C. M.; Fazio, D. D. Complementarity between Quantum and Classical Mechanics in Chemical Modeling. The $H + HeH^+ \longrightarrow H_2^+ + He$ Reaction: A Rigourous Test for Reaction Dynamics Methods. *J. Phys. Chem. A* **2015**, *119*, 12615.

(20) Stei, M.; Carrascosa, E.; Kainz, M. A.; Kelkar, A. H.; Meyer, J.; Szabó, I.; Czakó, G.; Wester, R. Influence of the leaving group on the dynamics of a gas-phase SN2 reaction. *Science* **2016**, *8*, 151.

(21) Bonnet, L.; Corchado, C.; Espinosa-Garcia, J. Pair-correlated speed distributions for the $OH+CH_4/CD_4$ reactions: Further remarks on their classical trajectory calculations in a quantum spirit. *C. R. Chimie* **2016**, *19*, 571.

(22) Shen, Z.; Ma, H.; Zhang, C.; Fu, M.; Wu, Y.; Bian, W.; Cao, J. Dynamical Importance of van der Waals Saddle and Excited Potential Surface in $C(^1D)+D_2$ Complex-Forming Reaction. *Nat. Commun.* **2017**, *8*, 14094.

(23) Bonnet, L.; Linguerri, R.; Hochlaf, M.; Yazidi, O.; Halvick, P.; Francisco, J. S. Full-Dimensional Theory of Pair-Correlated HNCO Photofragmentation. *J. Phys. Chem. Lett.* **2017**, *8*, 2420.

(24) Bonnet, L.; Espinosa-Garcia, J. Simulation of the experimental imaging results for the $OH + CHD_3$ reaction with a simple and accurate theoretical approach. *Phys. Chem. Chem. Phys.* **2017**, *19*, 20267.

(25) The previous references are obviously far from representing an exhaustive list.

(26) Karplus, M.; Porter, R.; Sharma, R. Exchange Reactions with Activation Energy. I. Simple Barrier Potential for (H, H$_2$). *J. Chem. Phys.* **1965**, *43*, 3259.

(27) Porter, R.; Raff, L. M. In ; Miller, W. H., Ed.; Dynamics of Molecular Collisions; Plenum, New York, 1976.

(28) Sewell, T.; Thomson, D. Classical Trajectory Methods for Polyatomic Molecules. *Int. J. Mod. Phys. B* **1997**, *11*, 1067.

(29) Lourderaj, U.; Park, K.; Hase, W. L. Classical trajectory simulations of post-transition state dynamics. *Int. Rev. Phys. Chem.* **2008**, *27*, 361.

(30) Brown, R. C.; Heller, E. J. Classical trajectory approach to photodissociation: The Wigner method. *J. Chem. Phys.* **1981**, *75*, 186.

(31) Schatz, G. Tunnelling in bimolecular collisions. *Chem. Rev.* **1987**, *81*, 87.

(32) Makri, N.; Miller, W. A Semiclassical Tunneling Model for Use in Classical Trajectory Simulations. *J. Chem. Phys.* **1989**, *91*, 4026.

(33) Guo, Y.; Thompson, D. A multidimensional semiclassical method for treating tunneling in molecular collisions. *J. Chem. Phys.* **1996**, *105*, 7480.

(34) Takatsuka, K.; Ushiyama, H.; Inoue-Ushiyama, A. Tunneling paths in multi-dimensional semiclassical dynamics. *Phys. Rep.* **1999**, *322*, 347.

(35) Xing, J.; Coronado, E.; Miller, W. Some New Classical and Semiclassical Models for Describing Tunneling Processes with Real-Valued Classical Trajectories. *J. Phys. Chem. B* **2001**, *105*, 6574.

(36) Rosa, C.; Brandao, J. Modelling tunnelling effects in multidimensional quasiclassical trajectories. Application to the O(3P) + H$_2$ reaction. *Chem. Phys. Lett.* **2008**, *461*, 150.

(37) Nakamura, H. Nonadiabatic chemical dynamics: Comprehension and control of dynamics, and manifestation of molecular functions. *Adv. Chem. Phys.* **2008**, *95*, 138.

(38) Barbatti, M. Nonadiabatic dynamics with trajectory surface hopping method. *Comp. Mol. Sci.* **2011**, *1*, 620.

(39) T. Yonehara, K. H.; Takatsuka, K. Fundamental approaches to nonadiabaticity: toward a chemical theory beyond the Born–Oppenheimer paradigm. *Chem. Rev.* **2012**, *112*, 499.

(40) Tully, J. *J. Chem. Phys.* **2012**, *137*, 22A301.

(41) Nakamura, H.; Nanbu, S.; Teranishi, Y.; Ohta, A. Development of semiclassical molecular dynamics simulation method. *Phys. Chem. Chem. Phys.* **2016**, *18*, 11972.

(42) Miller, W. H. Semiclassical Theory of Atom-Diatom Collisions: Path Integrals and the Classical S Matrix. *J. Chem. Phys.* **1970**, *53*, 1949.

(43) Miller, W. H. Classical S Matrix: Numerical Application to Inelastic Collisions. *J. Chem. Phys.* **1970**, *53*, 3578.

(44) Marcus, R. A. Extension of the WKB method to wave functions and transition probability amplitudes (S-matrix) for inelastic or reactive collisions. *Chem. Phys. Lett.* **1970**, *7*, 525.

(45) Marcus, R. A. Theory of Semiclassical Transition Probabilities (S Matrix) for Inelastic and Reactive Collisions. *J. Chem. Phys.* **1971**, *54*, 3965.

(46) Miller, W. H. Classical-limit quantum mechanics and the theory of molecular collisions. *Adv. Chem. Phys.* **1974**, *25*, 69.

(47) Miller, W. H. The Classical S-Matrix in Molecular Collisions. *Adv. Chem. Phys.* **1975**, *30*, 77.

(48) Heller, E. J. Uniform semiclassical IVR treatment of the S-matrix. *J. Chem. Phys.* **1975**, *62*, 1544.

(49) Campolieti, G.; Brumer, P. Semiclassical collision theory in the initial value representation: Efficient numerics and reactive formalism. *J. Chem. Phys.* **1992**, *96*, 5969.

(50) Shalashilin, D. V.; Jackson, B. Initial value representation for the classical propagator and S-matrix with the help of coherent states. *Chem. Phys. Lett.* **1998**, *291*, 143.

(51) van de Sand, G.; Rost, J. M. Uniform semiclassical IVR treatment of the S-matrix. *J. Phys. B* **2000**, *33*, 1423.

(52) Elran, Y.; Kay, K. G. Uniform semiclassical IVR treatment of the S-matrix. *J. Chem. Phys.* **2001**, *114*, 4362.

(53) Dasso, C. H.; Gallardo, M. I.; Saraceno, M. Semiclassical calculation of heavy-ion scattering in the chaotic regime. *Phys. Rev. C* **2007**, *75*, 054611.

(54) Bonnet, L.; Crespos, C. Phase-index problem in the semiclassical description of molecular collisions. *Phys. Rev. A* **2008**, *78*, 062713.

(55) Bonnet, L.; Crespos, C. Erratum: Phase-index problem in the semiclassical description of molecular collisions [Phys. Rev. A 78, 062713 (2008)]. *Phys. Rev. A* **2009**, *80*, 059903(E).

(56) Roueff, E.; Lique, F. Molecular Excitation in the Interstellar Medium: Recent Advances in Collisional, Radiative, and Chemical Processes. *Chem. Rev.* **2013**, *113*, 8906.

(57) de Lange, M. J. L.; Drabbels, M.; Griffiths, P. T.; Bulthuis, J.; Stolte, S.; Snijders, J. G. Steric asymmetry in state-resolved NO-Ar collisions. *Chem. Phys. Lett.* **1999**, *313*, 491.

(58) Alexander, M. H.; Stolte, S. Investigation of steric effects in inelastic collisions of NO($X^2\Pi$) with Ar. *J. Chem. Phys.* **2000**, *112*, 8017.

(59) Lorenz, K. T.; Chandler, D. W.; Barr, J. W.; Chen, W.; Barnes, G. L.; Cline, J. I. Direct Measurement of the Preferred Sense of NO Rotation After Collision with Argon. *Science* **2001**, *293*, 2063.

(60) Kohguchi, H.; Suzuki, T.; Alexander, M. H. Fully State-Resolved Differential Cross Sections for the Inelastic Scattering of the Open-Shell NO Molecule by Ar. *Science* **2001**, *294*, 832.

(61) Gijsbertsen, A.; Linnartz, H.; Taatjes, C. A.; Stolte, S. Quantum Interference as the Source of Steric Asymmetry and Parity Propensity Rules in NO-Rare Gas Inelastic Scattering. *J. Am. Chem. Soc.* **2006**, *128*, 8777.

(62) Eyles, C. J.; Brouard, M.; Yang, C.-H.; Klos, J.; Aoiz, F. J.; Gijsbertsen, A.; Wiskerke, A. E.; Stolte, S. Interference structures in the differential cross-sections for inelastic scattering of NO by Ar. *Nat. Chem.* **2011**, *3*, 597.

(63) von Zastrow, A.; Onvlee, J.; Vogels, S. N.; Groenenboom, G. C.; van der Avoird, A.; van de Meerakker, S. Y. T. State-resolved diffraction oscillations imaged for inelastic collisions of NO radicals with He, Ne and Ar. *Nat. Chem.* **2014**, *6*, 216.

(64) Nichols, B.; Chadwick, H.; Gordon, S. D. S.; Eyles, C. J.; Hornung, B.; Brouard, M.; Alexander, M. H.; Aoiz, F. J.; Gijsbertsend, A.; Stolte, S. Steric effects and quantum interference in the inelastic scattering of NO(X) + Ar. *Chem. Sci.* **2015**, *6*, 2202.

(65) Brouard, M.; Gordon, S. D. S.; Boyle, A. H.; Heid, C. G.; Nichols, B.; Walpole, V.; Aoiz, F. J.; Stolte, S. Integral steric asymmetry in the inelastic scattering of NO($X^2\Pi$). *J. Chem. Phys.* **2017**, *146*, 014302.

(66) McCurdy, C. W.; Miller, W. H. Interference effects in rotational state distributions: Propensity and inverse propensity. *J. Chem. Phys.* **1977**, *67*, 463.

(67) Arthurs, M.; Dalgarno, A. The theory of scattering by a rigid rotator. *Proc. R. Soc. London, Ser. A* **1960**, *256*, 540.

(68) Alexander, M. H. Quantum treatment of rotationally inelastic collisions involving molecules in Π electronic states: New derivation of the coupling potential. *Chem. Phys.* **1985**, *92*, 337.

(69) See also Ref.[56] and references therein.

(70) Semenov, A.; Babikov, D. Mixed quantum/classical theory of rotationally and vibrationally inelastic scattering in space-fixed and body-fixed reference frames. *J. Chem. Phys.* **2013**, *139*, 174108.

(71) Semenov, A.; Babikov, D. Mixed Quantum/Classical Approach for Description of Molecular Collisions in Astrophysical Environments. *J. Phys. Chem. Lett.* **2015**, *6*, 1854.

(72) Babikov, D.; Semenov, A. Recent Advances in Development and Applications of the Mixed Quantum/Classical Theory for Inelastic Scattering. *J. Phys. Chem. A* **2016**, *120*, 319.

(73) Semenov, A.; Babikov, D. Three sources of errors in the Ehrenfest treatment of inelastic scattering and possible ways of resolving them. *J. Chem. Phys.* **2017**, *146*, 224107.

(74) Miller, W. H. Classical S Matrix for Rotational Excitation; Quenching of Quantum Effects in Molecular Collisions. *J. Chem. Phys.* **1971**, *54*, 5386.

(75) Skodje, R. T. On the use of the interaction picture in classical mechanics. *Chem. Phys. Lett.* **1984**, *109*, 221.

(76) Littlejohn, R. G. The Van Vleck Formula, Maslov Theory, and Phase Space Geometry. *J. Stat. Phys.* **1992**, *68*, 7.

(77) Gutzwiller, M. C. *Chaos in Classical and Quantum Mechanics*; Springer-Verlag, New York, 1990.

(78) Campolieti, G.; Brumer, P. Semiclassical propagation: Phase indices and the initial-value formalism. *Phys. Rev. A* **1994**, *50*, 997.
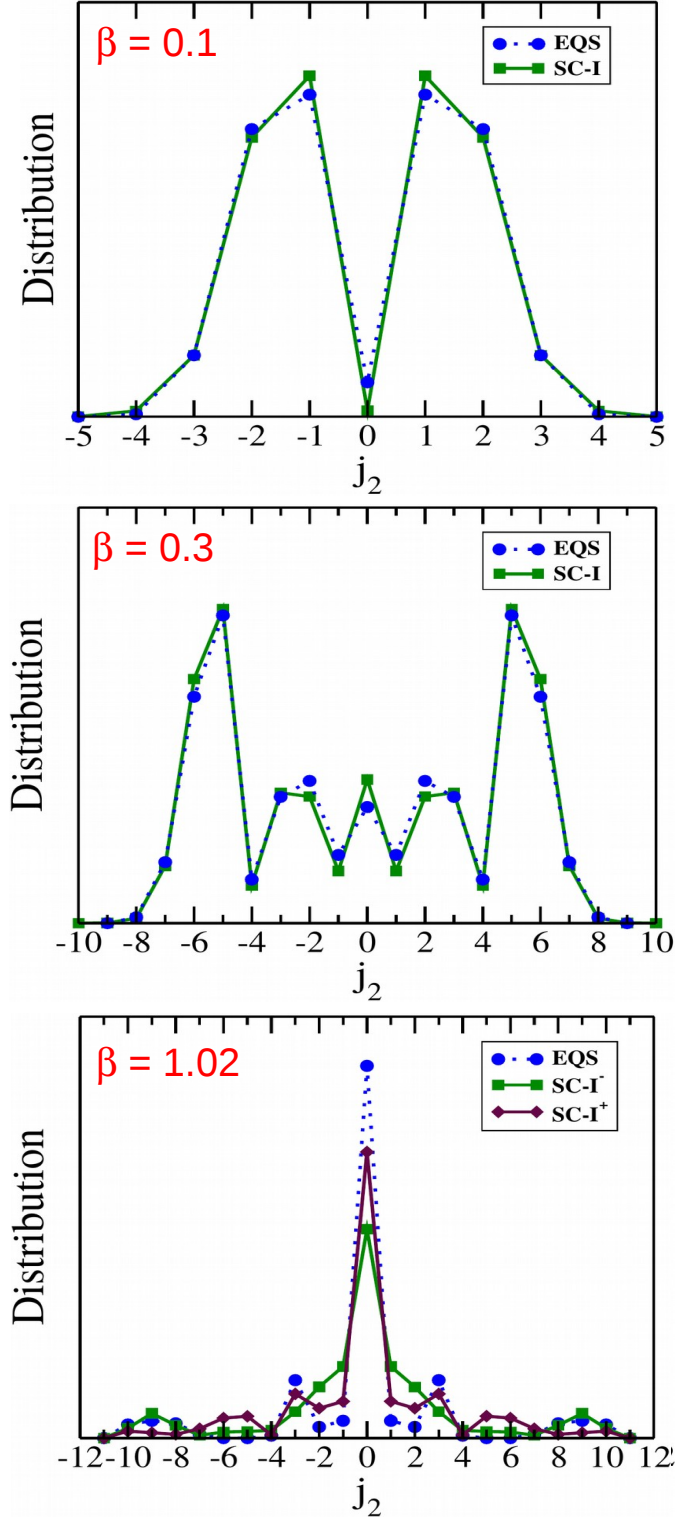
Figure 1: Rotational state distributions found from exact quantum scattering (EQS) calculations (blue circles connected by dotted segments) and semiclassical calculations according to Eq. (11) (green squares or brown diamonds connected by solid segments). Three different values of the β parameter are considered in Eq. (12). The acronyms SC-I, SC-I$^-$ and SC-I$^+$ correspond to different definitions of the index ν in Eq. (11) (see text).
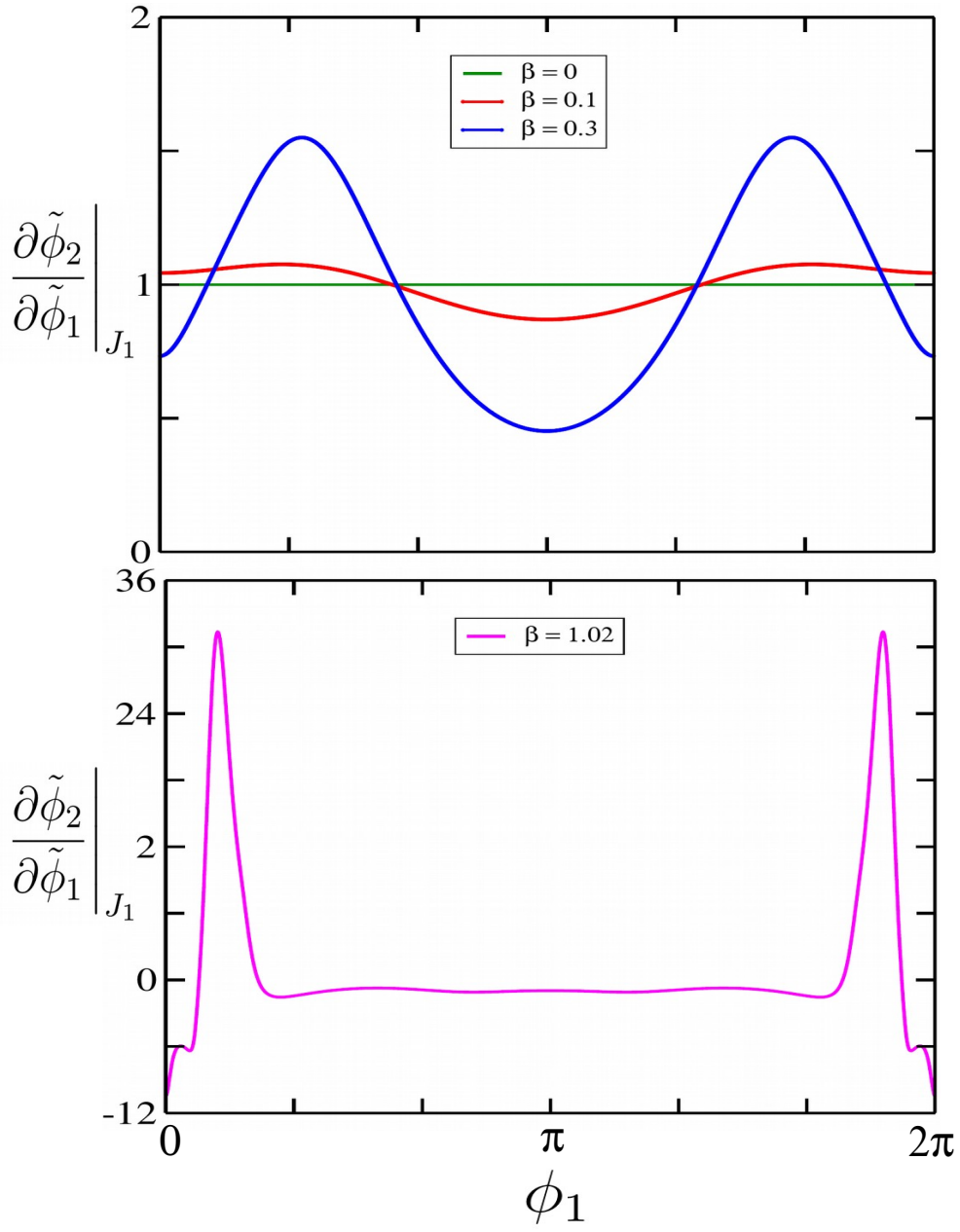
Figure 2: $\left.\frac{\partial \tilde{\phi}_2}{\partial \tilde{\phi}_1}\right|_{J_1}$ in terms of ϕ_1 $(= \tilde{\phi}_1)$ for β equal 0, 0.1 and 0.3 (upper panel) and 1.02 (lower panel).
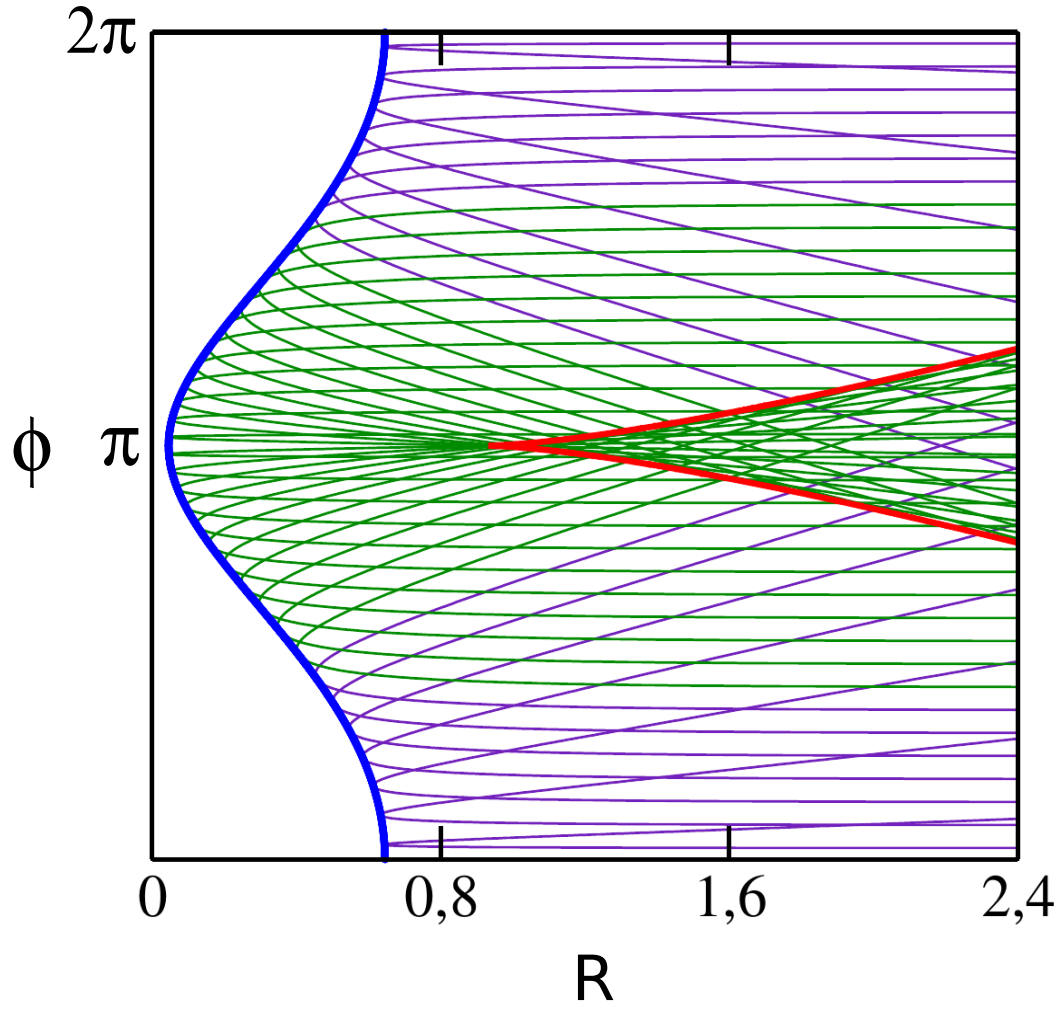
Figure 3: Set of 36 trajectories for $\beta = 0.3$. Indigo paths touch only one caustic, represented in blue, while green paths touch both the previous caustic and a second one represented in red (see text for more details).
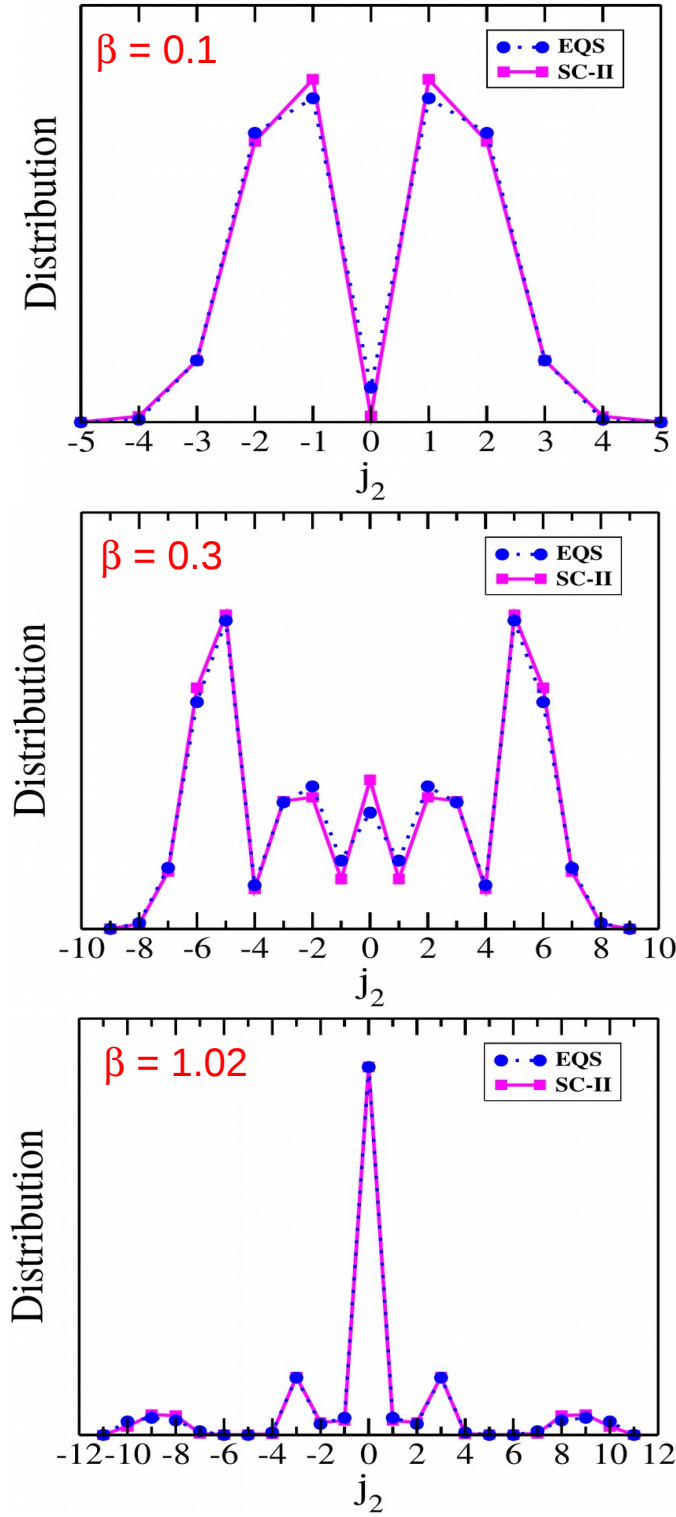
Figure 4: Rotational state distributions found from exact quantum scattering (EQS) calculations (blue circles connected by dotted segments) and semiclassical (SC-II) calculations according to Eq. (28) (magenta squares connected by solid segments).
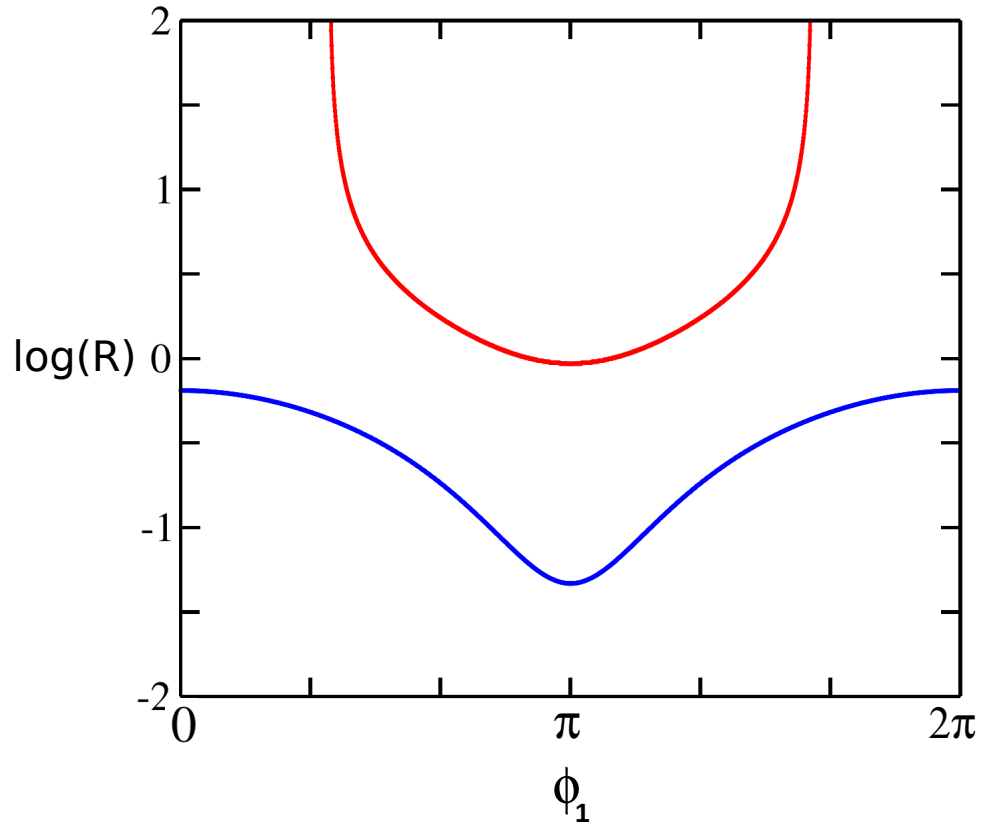
29

Figure 5: Values of $log(R)$ in terms of ϕ_1 at the blue and red caustics (see Fig. 3 for their representation in the (R, ϕ) plane).
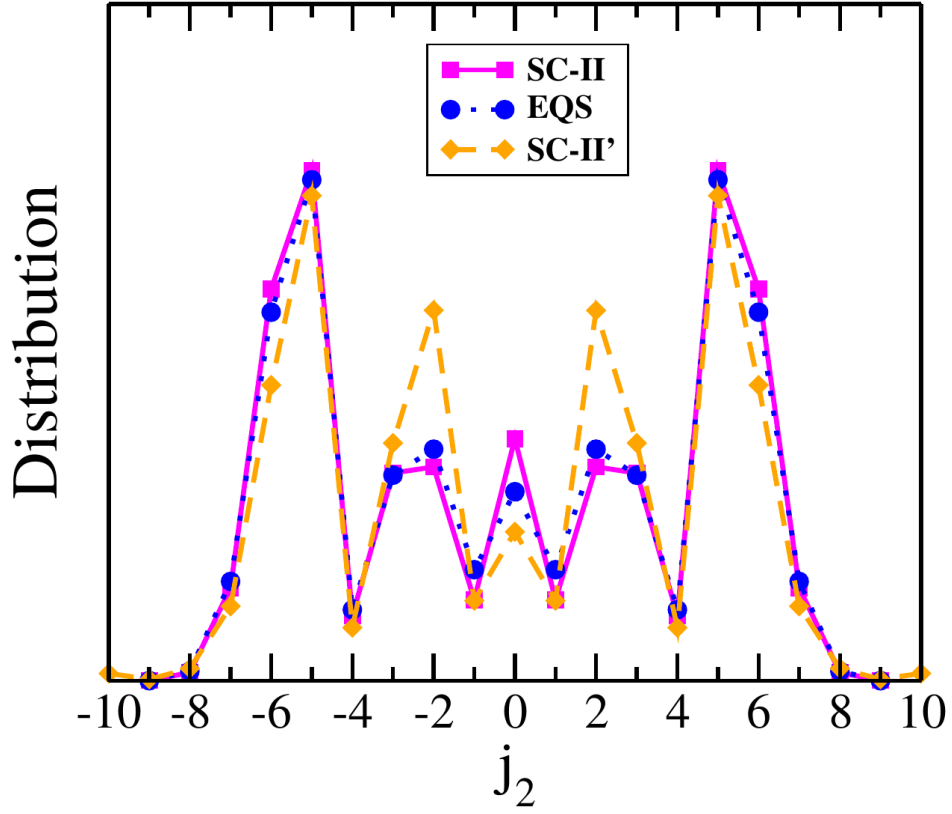
Figure 6: Rotational state distributions found from exact quantum scattering (EQS) calculations (blue circles connected by dotted segments), converged semiclassical (SC-II) calculations according to Eq. (28) for $R_2 = 10^3$ Å (magenta squares connected by solid segments), and non converged semiclassical (SC-II') calculations according to Eq. (28) for $R_2 = 10$ Å (orange diamonds connected by dashed segments).